UNVEILING THE NATURE OF IGR J17177–3656 WITH X-RAY, NEAR-INFRARED, AND RADIO OBSERVATIONS

The Astrophysical Journal, 738:183 (8pp), 2011 September 10 doi:10.1088/0004-637X/738/2/183

UNVEILING THE NATURE OF IGR J17177−3656 WITH X-RAY, NEAR-INFRARED, AND RADIO OBSERVATIONS

A. Paizis[1], M. A. Nowak[2], J. Wilms[3], S. Chaty[4], S. Corbel[4], J. Rodriguez[4], M. Del Santo[5], P. Ubertini[5], and R. Chini[6,7]

[1] Istituto Nazionale di Astrofisica, INAF-IASF, Via Bassini 15, I-20133 Milano, Italy; ada@iasf-milano.inaf.it
[2] Massachusetts Institute of Technology, Kavli Institute for Astrophysics, Cambridge, MA 02139, USA; mnowak@space.mit.edu
[3] Dr. Karl Remeis-Sternwarte and Erlangen Centre for Astroparticle Physics, Universität Erlangen-Nürnberg, Sternwartstr. 7, D-96049 Bamberg, Germany
[4] AIM-Astrophysique, Instrumentation et Modélisation (UMR-E 9005 CEA/DSM-CNRS-Université Paris Diderot) Irfu/Service d'Astrophysique, Centre de Saclay, F-91191 Gif-sur-Yvette Cedex, France
[5] IASF Roma-INAF, Via del Fosso del Cavaliere 100, I-00133 Roma, Italy
[6] Astronomisches Institut, Ruhr-Universität Bochum, Universitätsstraße 150, D-44780 Bochum, Germany
[7] Instituto de Astronomía, Universidad Católica del Norte, Avenida Angamos 0610, Casilla 1280, Antofagasta, Chile
Received 2011 May 27; accepted 2011 June 25; published 2011 August 25

ABSTRACT

We report on the first broadband (1–200 keV) simultaneous *Chandra–INTEGRAL* observations of the recently discovered hard X-ray transient IGR J17177−3656 that took place on 2011 March 22, about two weeks after the source discovery. The source had an average absorbed 1–200 keV flux of about 8×10^{-10} erg cm^{-2} s^{-1}. We extracted a precise X-ray position of IGR J17177−3656, $\alpha_{J2000} = 17^{h}17^{m}42\overset{s}{.}62$, $\delta_{J2000} = -36^{\circ}56'04\overset{''}{.}5$ (90% uncertainty of $0\overset{''}{.}6$). We also report *Swift*, near-infrared, and quasi-simultaneous radio follow-up observations. With the multi-wavelength information at hand, we propose IGR J17177−3656 is a low-mass X-ray binary, seen at high inclination, probably hosting a black hole.

Key words: accretion, accretion disks – binaries: close – stars: individual (IGR J17177–3656) – X-rays: binaries

Online-only material: color figures

1. INTRODUCTION

On 2011 March 15 (MJD 55635), *INTEGRAL* (*INTErnational Gamma-Ray Astrophysics Laboratory*) discovered the new hard X-ray transient IGR J17177−3656 (Frankowski et al. 2011). The IBIS/ISGRI spectrum (20–200 keV) could be well described by a power law with photon index 1.8 ± 0.3 and a flux of about 20 mCrab. The source was also marginally detected in JEM-X in the 10–20 keV band (about 8 mCrab) but was not detected in the 3–10 keV band with a 3σ upper limit of 5 mCrab.

Following the *INTEGRAL* discovery, a *Swift* target of opportunity (ToO) was performed on 2011 March 16 (Zhang et al. 2011). A refined *Swift* position was reported (90% uncertainty of $2\overset{''}{.}1$), consistent with the *INTEGRAL* one. A combined, though non-simultaneous, *Swift*/X-ray telescope (XRT) and *INTEGRAL*/IBIS/ISGRI spectral fit with an absorbed power-law model yielded $N_{H} = 3.9^{+0.5}_{-0.4} \times 10^{22}$ cm^{-2} and photon index $\Gamma = 1.5 \pm 0.2$, indicating a hard state with additional absorbing column density intrinsic to the source (Zhang et al. 2011). Based on the *Swift* position and uncertainty, a search through the VizieR database resulted in only one match: 2MASS J17174269−3656039 ($K = 12.9$) located at about $1\overset{''}{.}3$ from the *Swift* position of Zhang et al. (2011).

Our *Chandra* ToO was performed on 2011 March 22, and thanks to the excellent *Chandra* location accuracy, an X-ray source position with a $0\overset{''}{.}6$ (90%) uncertainty was reported (Paizis et al. 2011). The new *Chandra*-based position, not consistent with the *Swift* one (∼$4\overset{''}{.}8$ away, but see Section 3.4), probably ruled out the Two Micron All Sky Survey (2MASS) association ($1\overset{''}{.}05$ away) and allowed the scientific community as well as members of our team to search for near-infrared (NIR) and radio counterparts (this paper; Corbel & Tzioumis 2011; Torres et al. 2011; Rojas et al. 2011).

The nature of IGR J17177−3656 is still to be unveiled and in this paper we describe our multi-wavelength campaign and contribution to its investigation.

2. MULTI-WAVELENGTH OBSERVATIONS

We present a detailed broadband analysis of the recently discovered IGR J17177−3656[8] using our *Chandra* ToO data and simultaneous higher energy *INTEGRAL* data. To obtain an overall view of the behavior of IGR J17177−3656, we have also analyzed available *Swift* and *INTEGRAL* monitoring data relevant to our investigation. Given our *Chandra* position, we triggered NIR observations to look for possible counterparts to IGR J17177−3656. These data are included in this paper, as well as the quasi-simultaneous radio observation reported by Corbel & Tzioumis (2011).

2.1. Chandra Data

We observed IGR J17177−3656 for 20 ks with *Chandra* on 2011 March 22, from 06:07:15 UT until 12:00:48 UT (MJD 55642, ObsID 12452) with the High Energy Transmission Grating Spectrometer (HETGS; Canizares et al. 2000) collecting high-resolution spectral information with the High Energy Grating (HEG), 0.8–10 keV, and Medium Energy Grating (MEG), 0.4–8.0 keV. The data were analyzed in a standard manner using the CIAO version 4.3 software package and *Chandra* CALDB version 4.4.2. The spectra were analyzed with the `ISIS` analysis system, version 1.6.1 (Houck 2002).

2.2. INTEGRAL Data

Starting from its discovery, IGR J17177−3656 has been in the *INTEGRAL*/IBIS (Ubertini et al. 2003) field of view during the

[8] See http://irfu.cea.fr/Sap/IGR-Sources/ for a regularly updated list of *INTEGRAL* sources.

Galactic bulge monitoring[9] (Kuulkers et al. 2007), as well as during the inner disk ($l < 0$) observations. A complete study of these *INTEGRAL* data is out of the scope of this paper. We will focus on the simultaneous *Chandra*/HETGS–*INTEGRAL*/IBIS set, in the first simultaneous broadband study of IGR J17177−3656. To properly understand the long-term hard X-ray behavior of the source (>20 keV) however, we have analyzed the IBIS/ISGRI data (20–600 keV; Lebrun et al. 2003) starting from revolution 1028 (2011 March 15, 09:23:08 UT, MJD 55635.39) to revolution 1032 (2011 March 28, 22:16:46 UT, MJD 55648.93), spanning a period of about 14 days. A standard analysis using version 9.0 of the Off-line Scientific Analysis (OSA) software was performed.

2.3. Swift Data

The 2011 outburst of IGR J17177−3656 was monitored with a total of eight daily pointed observations with the *Swift* X-Ray Reflecting Telescope (Burrows et al. 2005; Gehrels et al. 2004) between 2011 March 16 and 23. Exposure times varied between 2 ks and 8 ks. The data were processed using the newest version of the *Swift* data analysis pipelines in HEASOFT 6.10. After re-processing the data with `xrtpipeline`, spectra were extracted with `xselect` using XRT grades 0 through 12. We used the newest XRT response matrix available in CALDB. Ancillary response matrices were generated using `xrtmkarf`, taking vignetting effects into account.

In addition to these data, IGR J17177−3656 was in the field of view of a 560 s long XRT pointing taken on 2011 January 27, but it was not detected during that observation.

2.4. Radio Data

We conducted continuum radio observations with the Australia Telescope Compact Array (ATCA) located in Narrabri, New South Wales, Australia. The ATCA synthesis telescope is an east–west array consisting of six 22 m antennas. The ATCA uses orthogonal polarized feeds and records full Stokes parameters. We carried out the observations with the upgraded Compact Array Broadband Backend, which provides a new broadband backend system for the ATCA and increases the maximum bandwidth from 128 MHz to 2 GHz.

The ATCA observations were conducted on the same day as the *Chandra* observations, 2011 March 22, at two frequency bands simultaneously, with central frequencies at 5.5 GHz and 9 GHz. The ATCA was in the intermediate 1.5A configuration. A total observation time of 0.66 hr on source was obtained for IGR J17177−3656. The amplitude and bandpass calibrator was PKS 1934−638, and the antenna's gain and phase calibration, as well as the polarization leakage, were derived from regular observations of the nearby (∼2.°9 away) calibrator PMN 1714−336. The editing, calibration, Fourier transformation, deconvolution, and image analysis were performed using the `MIRIAD` software package (Sault et al. 1995; Sault & Killeen 2006). The cleaning process was carried out using a combination of multi-frequency (Sault & Wieringa 1994) and standard clean algorithms.

2.5. Near-infrared Data

Near-infrared K_s observations were performed at the Universitätssternwarte Bochum near Cerro Armazones in the Chilean Atacama desert. We used the 80 cm IRIS telescope equipped with a 1024 × 1024 pixels HAWAII-1 detector array (Hodapp et al. 2010). The observational sequence consisted of eight exposures between MJD 55647.38 and 55647.40 (2011 March 27, 09:10:50 < UT < 09:38:36) each comprising conventional dithering and chopping patterns to allow subtraction of the bright NIR sky. The total on-source integration time was 400 s. Data reduction involved standard IRAF procedures; astrometry and photometric calibration were achieved via 1958 sources from the 2MASS archive.

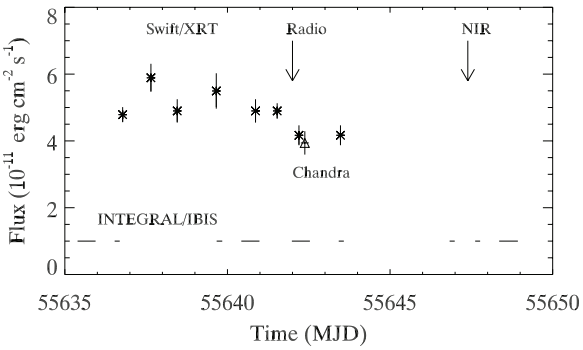

Figure 1. IGR J17177−3656 *Swift* and *Chandra* (absorbed) flux evolution in the 2–8 keV range. For clarity the *INTEGRAL* coverage of the source is also shown, marked as horizontal lines, together with our NIR and radio follow-up observations, as discussed in this paper.

3. RESULTS

An overview of all the data treated in this paper is shown in Figure 1. The absorbed 2–8 keV flux evolution of IGR J17177−3656 as seen by *Swift* is shown together with our *Chandra* average data point.[10] The *INTEGRAL* coverage of the source is marked as horizontal lines. Finally, the time of our NIR observation and the time of the radio observation included in this work are also shown.

3.1. Chandra Position, Variability, and Spectra

We extracted the X-ray position of IGR J17177−3656 from the zeroth-order image, obtaining $\alpha_{J2000} = 17^h17^m42\overset{s}{.}62$, $\delta_{J2000} = -36°56'04\overset{''}{.}5$ (Paizis et al. 2011). Given the brightness of the source, the statistical error is smaller than the absolute position accuracy of *Chandra*, 0.″6 at 90% uncertainty.[11] Therefore, we attribute a 90% uncertainty of 0.″6 to the position found.

In Paizis et al. (2011), we performed a simple phenomenological fit to the MEG and HEG first-order grating spectra. The *Chandra* total (about 20 ks) spectrum was consistent with an absorbed power law with a column density of approximately $N_H = (5.9 \pm 1.5) \times 10^{22}$ cm^{-2} (90% confidence) and photon index $\Gamma = 1.2 \pm 0.4$ (90% confidence) with the source at about a 3 mCrab flux level in the 2–10 keV range. The *Chandra* spectrum alone is very hard but this is likely due to the narrow energy range in which the fit is performed, which is strongly absorbed at lower energies by the heavy intrinsic absorbing column density present in the source.

A detailed analysis of the source light curve, with 200 s time bins, showed variability; hence we cut the data in three, non-contiguous, intervals: a 2–8 keV rate <40 counts bin^{-1}

[9] http://isdc.unige.ch/Science/BULGE/

[10] The absorbed flux is shown, which we believe to be a more solid indication of the source state given its heavy intrinsic and variable absorbing column density.

[11] http://cxc.harvard.edu/cal/ASPECT/celmon/

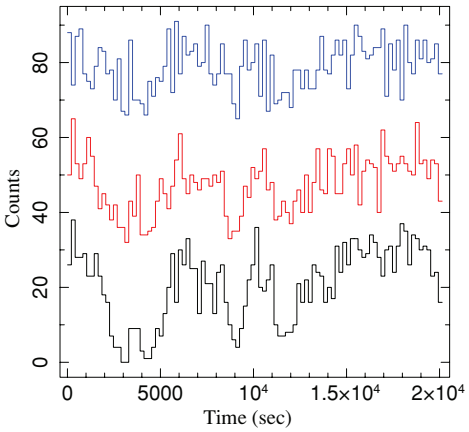

Figure 2. 200 s light curves in three energy bands: 2–3.7 keV (black), 3.7–4.7 keV (red), and 4.7–8 keV (blue). For visualization purposes, the middle (red) and high band (blue) are offset by 30 and 60 counts with respect to the low (black) band.

(A color version of this figure is available in the online journal.)

(*Chandra*-low, 4.6 ks), between 40 and 60 counts bin^{-1} (*Chandra*-mid, 4.5 ks), and >60 counts bin^{-1} (*Chandra*-high, 10.4 ks).

For each of the three intervals, we extracted again the first-order dispersed spectra ($m = \pm 1$ for HEG and MEG), and to increase the signal-to-noise ratio we merged the two HEG ($m = \pm 1$) and MEG ($m = \pm 1$) spectra into one combined spectrum, for a total of three spectra (one per rate level).[12] Final binning, starting at 0.8 keV, was chosen to have a signal-to-noise ratio higher than 5 and a minimum of 16 MEG channels per bin. The fitting results of these three spectra are given in Section 3.3 together with the simultaneous *INTEGRAL*/IBIS one.

Figure 2 shows the 200 s light curve in three energy bands 2–3.7 keV (black), 3.7–4.7 keV (red), and 4.7–8 keV (blue). The bands were chosen to have roughly equal integrated counts and for visualization purposes the light curves are respectively offset by 30 and 60 counts for the middle (red) and high (blue) band with respect to the low (black) band. As can be seen, the variability is more evident in the softer band: see, e.g., the large dip-like structure right before 5000 s where the flux becomes undetectable in one 200 s bin. Generally the lower the total counts, the harder the source (due to, for example, increasing absorbing column density and/or spectral slope change).

3.2. *INTEGRAL* Non-variability and Spectrum

For all the *INTEGRAL* coverage shown in Figure 1, we extracted images in the 17–50 keV energy band (one image per pointing) to search for possible source flares. Among the 121 pointings analyzed, only in three was the source detected at a single pointing level (detection significance $>5\sigma$). This result shows that in a single pointing IGR J17177−3656 is (at best) at the detection limit in IBIS/ISGRI, corresponding to about 25 mCrab in a 1 ks pointing.[13] Hence for the spectral analysis we decided to extract the source spectrum from the mosaics (where the detection significance is higher, using the *mosaic_spec* tool available in the OSA package), rather than on a single pointing basis. A second run was thus made to extract images in the 20.18–30.23, 30.23–49.6, 49.6–100.12, and 100.12–200.17 keV bands (the energy boundaries are given by the response matrix itself). This spectral extraction was made *only* for the data that were *simultaneous* to the *Chandra* 2011 March 22 ToO (∼20 ks).

[12] The *Chandra* zeroth order, that qualitatively verifies the source flux variability, was not used in the spectral analysis as it suffers from pileup.

[13] The higher detection significance quoted in the discovery ATel (Frankowski et al. 2011) is obtained by mosaicking different pointings.

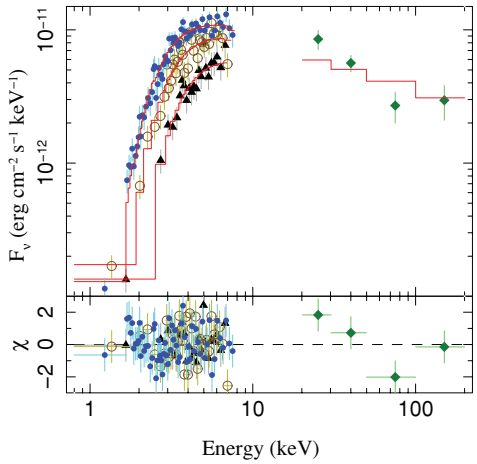

Figure 3. Spectral model of Table 1.

(A color version of this figure is available in the online journal.)

Given the three luminosity levels detected in *Chandra* data (Section 2.1), we extracted three spectra also for IBIS/ISGRI, matching as closely as possible the non-consecutive *Chandra*-low, -mid, and -high times. This resulted in about 4.3 ks for *INTEGRAL*-low (as opposed to 4.6 ks for *Chandra*-low), about 4.3 ks for *INTEGRAL*-mid (4.5 ks for *Chandra*-mid), and about 9.6 ks for *INTEGRAL*-high (10.4 ks for *Chandra*-high). The small differences in final integration times are due to the fact that whereas *Chandra* has a continuous observation, *INTEGRAL* is dithering and hence the slew times between re-pointing are lost.

The three spectra do not show any variability: IBIS/ISGRI is not capable of disentangling the three states due to the short integration time and low statistics. Alternatively, we are seeing the extension of the trend of Figure 2, i.e., as we move to harder X-rays, the source is less variable. Indeed the three IBIS/ISGRI spectra have comparable normalization and slope ($\Gamma_{\rm Low} = 1.8^{+0.5}_{-1.4}$, $\Gamma_{\rm Mid} = 1.9^{+0.8}_{-1.1}$, $\Gamma_{\rm High} = 1.8^{+0.5}_{-0.6}$). Furthermore, we note that the IBIS/ISGRI spectrum reported in the discovery ATel of IGR J17177−3656 by Frankowski et al. (2011) (2011 March 15) could also be well described by a power law with photon index 1.8 ± 0.3; hence the hard X-rays did not experience a significant evolution from March 15 to March 22.

3.3. *Chandra*–*INTEGRAL* Simultaneous Spectra

Since IGR J17177−3656 does not show any appreciable variability in the IBIS/ISGRI range (>20 keV), to increase statistics we extract the IBIS/ISGRI average spectrum that is shown in Figure 3, together with the three *Chandra* spectra (low, mid, high). The spectral model used to fit the combined spectrum is shown in Table 1. A cross-normalization constant ($C_{\rm cn}$) was allowed between *Chandra*-grating and *INTEGRAL*/IBIS and was set to 1 for *Chandra* and free for *INTEGRAL*. Beside the interstellar medium (ISM) absorbing column density fixed to 1.5×10^{22} cm^{-2}, a clearly varying local column density is needed, from 7.0×10^{22} cm^{-2} in *Chandra*-high to 16.8×10^{22} cm^{-2} in *Chandra*-low (higher absorption, lower *Chandra* rate).

In the fit we have used an improved model for the absorption of X-rays in the ISM by Wilms et al. (2000) (so-called `tbabs`).

Table 1
Fits to IGR J17177−3656 Spectra: C_{cn}*(TBnew(*ISM*)*((TBnew(*local*)+C_f)*powerlaw))

Instrument	N_H (10^{22} cm^{-2})	C_f	Γ	2–8 keV Flux[a] ($\times10^{-11}$ erg cm^{-2} s^{-1})	20–200 keV Flux[b] ($\times10^{-10}$ erg cm^{-2} s^{-1})	C_{cn}	χ^2/dof
Chandra-low	$16.8^{+3.5}_{-3.1}$	$0.015^{+0.009}_{-0.019}$	$1.36^{+0.16}_{-0.15}$	$2.36^{+0.19}_{-0.19}$	...	1	130.9/111
Chandra-mid	$10.5^{+1.7}_{-1.5}$	$0.013^{+0.008}_{-0.010}$	...	$4.03^{+0.23}_{-0.22}$	...	1	...
Chandra-high	$7.0^{+0.9}_{-0.8}$	$0.00^{+0.010}_{-0.000}$	...	$5.44^{+0.20}_{-0.19}$	...	1	...
IBIS/ISGRI	...	...	...	...	$6.48^{+0.94}_{-1.15}$	$0.79^{+0.50}_{-0.26}$	

Notes. Errors are 90% confidence level for one parameter. N_H is the neutral column density *local to the system*. The ISM interstellar column density has been fixed to 1.5×10^{22} cm^{-2}. C_f is a dimensionless constant to allow for partial covering (covering fraction $\equiv (1 + C_f)^{-1}$). Γ is the power-law photon index, which was constrained to be the same for all data sets. For the IBIS/ISGRI data, all model parameters have been tied to those of the *Chandra*-high data set. We have further allowed for a cross-normalization constant, C_{cn}, for the IBIS/ISGRI detector. (This cross-normalization also subsumes the intrinsic flux variation of the *Chandra* spectra.)

[a] Absorbed flux, relative to the *Chandra* response.

[b] Relative to the IBIS/ISGRI response and includes the cross-normalization constant.

Such a model results in higher column densities with respect to, e.g., the `wabs` model of Morrison & McCammon (1983). Indeed in the earlier ISM absorption models, the abundances assumed for the ISM were the solar ones, while more abundance measurements outside the solar system showed that the total gas plus dust ISM abundances are actually lower than the solar abundances. Hence, with this correction, a higher column density is needed for a given spectrum (Wilms et al. 2000, and references therein). For this reason, the absorbing column density of Paizis et al. (2011), which was determined from solar abundances, differs from the one given here.

During the fitting process it became clear that variability of N_H alone would not be enough to explain the *Chandra* variability. Specifically, we noted that the spectral models that let free the neutral column density alone left positive residuals in the 0.8–3 keV band, especially during the most absorbed phase. Though this soft excess could be modeled in a number of ways, utilizing a partial covering fraction seems a natural hypothesis. These factors, although small (*Chandra*-low $C_f = 0.015$ and *Chandra*-mid $C_f = 0.013$), improved the χ^2 by 12. C_f was not applied to IBIS/ISGRI (>20 keV).

Given that the spectral slope does not show dramatic changes neither in the *INTEGRAL*/IBIS spectra already discussed nor in the *Swift* ones (see the next section), in our fit the power-law photon index Γ was constrained to be the same for all data sets, letting the soft X-ray flux variability be explained by intrinsic N_H and (slight) covering. Figure 4 shows that care has to be taken for the final value of the spectral slope since it clearly depends on the *Chandra–INTEGRAL* cross-normalization. We note that trying to describe the broadband data with a variable slope and fixed column density led to a very hard spectral index, Γ down to 0.7, and cross-normalization $C_{cn} = 0.5$, i.e., the slope appeared to be too hard for IBIS/ISGRI, and its amplitude had to be halved to make the fit. Although we cannot rule out a contribution of the spectral slope to the overall variability, we assume the simplest model (fixed Γ, variable local N_H). Finally, we note that a cutoff power law is not strongly preferred (χ^2/dof = 126.8/109), leading to an unconstrained cutoff energy of $E_c > 34$ keV.

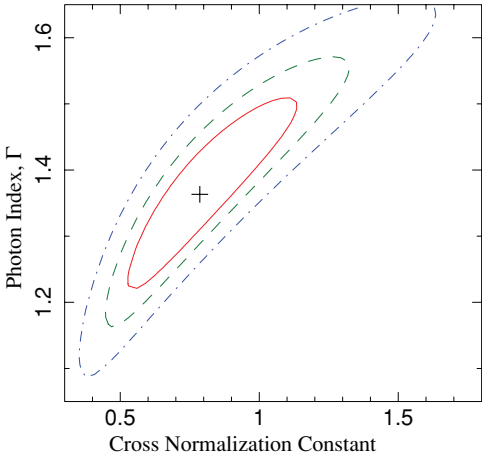

Figure 4. Contours of IBIS/ISGRI normalization constant vs. photon index. (68%, 90%, and 99% confidence for two parameters.)

(A color version of this figure is available in the online journal.)

3.4. Swift Position and Average Spectrum

The position of IGR J17177−3656 determined from the summed image of the whole *Swift* campaign is $\alpha_{J2000} = 17^h17^m42\overset{s}{.}4$, $\delta_{J2000} = -36°56'03\overset{''}{.}6$ with a formal uncertainty estimated to 3″. We note that in the first *Swift* observation the image of IGR J17177−3656 was distorted by a chip gap, causing an offset in the first *Swift* position reported by Zhang et al. (2011) and the position reported here. Our inferred *Chandra* and *Swift* positions are consistent (2.″8 away).

A spectral analysis of the observations shown in Figure 1 has been performed. As for the *INTEGRAL* long-term data, a detailed analysis and discussion of the *Swift* results is out of the scope of the paper. The spectra of the *Swift*/XRT data alone can be well described with an absorbed power law throughout all the monitoring shown in Figure 1. The flux variability is less than a factor of two, the spectral slope is constant within 90% error bars, while there seems to be an increase in the absorbing column density in the last *Swift* point of Figure 1, just after our *Chandra* observation (i.e., the last point is not within 90% error bars, but still within 99%). To have a global spectral view of the *Swift* results, since IGR J17177−3656 does not show any significant variability in the *Swift* data, we co-added the single available spectra and fitted the overall *Swift* spectrum (total exposure of about 16 ks) using the same model structure of Section 3.3. We obtain a local absorbing column density $N_H = 6.5^{+0.6}_{-0.8} \times 10^{22}$ cm^{-2}, $\Gamma = 1.7^{+0.2}_{-0.1}$, covering factor $C_f = 0.015^{+0.007}_{-0.008}$, and absorbed 2–8 keV flux $F = (4.4 \pm 0.1) \times 10^{-11}$ erg cm^{-2} s^{-1} (141.4/141 χ^2/dof). The average spectrum and fit are shown in Figure 5.

The N_H value obtained from the average *Swift* spectrum is not compatible with the average *Chandra–INTEGRAL* values and

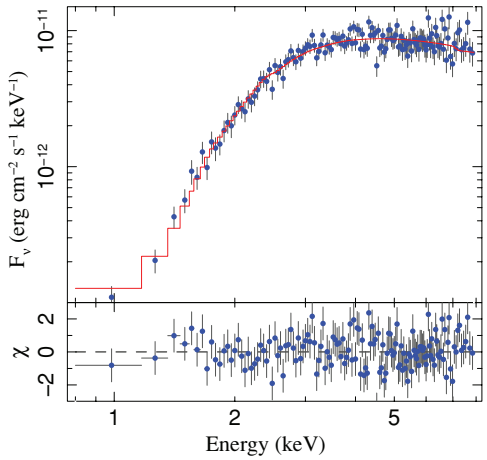

Figure 5. *Swift* average spectrum of IGR J17177−3656. See the text for details. (A color version of this figure is available in the online journal.)

is in fact only compatible with the least absorbed phases of the *Chandra* spectrum (*Chandra*-high).

Similarly the *Swift* slope is 1.7 rather than around 1.4 for *Chandra–INTEGRAL*. We note however that the slope difference (and in turn $N_{\rm H}$) could be due to the fact that the *Swift* fit performed here is not coupled to the *INTEGRAL* data (as is *Chandra*). Zhang et al. (2011), when fitting together (non-simultaneous) *Swift* and *INTEGRAL* data, obtain a spectral slope $\Gamma = 1.5 \pm 0.2$ (consistent with our result), albeit using a different absorption model than ours.

We emphasize that an accurate comparison cannot be done without a further investigation in the *Swift*, *Chandra*, and *INTEGRAL* cross-normalization constants. Even within the *Swift* data alone, in order to establish a solid variability in the absorbing column density, a deeper study is required, e.g., selecting different count-rate states from finer binning light curves, extracting average spectra and comparing them, as done for *Chandra* in this work.

3.5. Radio

Figure 6 shows the radio map obtained using the combined ATCA observations of IGR J17177−3656 at 5.5 and 9 GHz. Contours are at −3, 3, 4, 5, and 6 times the rms noise level of 48 μJy beam^{-1}. The synthesized beam (in the lower right corner) is $6\farcs0 \times 1\farcs6$, with the major axis at a position angle of $42\fdg3$. The ATCA data indicate the presence of a single radio source within the *Chandra* X-ray error circle with measured flux densities of 0.24 ± 0.06 mJy at 5.5 GHz and 0.20 ± 0.06 mJy at 9 GHz. The poorly constrained spectral index obtained is $\alpha = -0.37 \pm 0.79$.

The most accurate localization of the radio counterpart is obtained by combining the two frequency data sets, giving a location of the radio source of $\alpha_{\rm J2000} = 17^{\rm h}17^{\rm m}42\fs59$, $\delta_{\rm J2000} = -36\degr56'04\farcs4$ ($0\farcs5$, 1σ positional uncertainty). Given its location coincident with the *Chandra* one ($0\farcs37$ away, Figure 6), it likely corresponds to the radio counterpart of IGR J17177−3656, though variability at radio frequencies would be needed to clearly establish this association.

3.6. Near-infrared

The final averaged $K_{\rm s}$ image of the field of view around IGR J17177−3656 is shown in Figure 7 and displays sources down to $K_{\rm s} = 16.3$ mag.

The closest visible star to our obtained *Chandra* position, visible in the figure, is the already mentioned 2MASS J17174269−3656039 that seems to be blended with a weaker source. This blended doublet is present both in recent (2011 March 27, this paper and 2001 March 20, Torres et al. 2011) and archival NIR maps (2010 April and October, Rojas et al. 2011). As already stated, the overall 90% uncertainty circle of the *Chandra* X-ray absolute position has a radius of $0\farcs6$, while the 99% limit on positional accuracy is $0\farcs8$ with the worst case offset being 1.1. 2MASS J17174269−3656039 is $1\farcs05$ away from our position while the weaker source is $0\farcs9$. These separations are very small and they may not rule out categorically the association with either source. However, assuming that the single radio source mentioned in Section 3.5, compatible with the *Chandra* position ($0\farcs37$ away), corresponds to the right counterpart, then the radio position would also tend to rule out 2MASS J17174269−3656039 and the faint infrared star. Furthermore, as already pointed out by Torres et al. (2011), even taking the *Swift* absorption that is lower than *Chandra–INTEGRAL* one would lead to $(J - K) \sim 6$ that is higher than what is obtained for the blended sources (Torres et al. 2011; Rojas et al. 2011). It is reasonable to conclude that no IR source is visible either in the $0\farcs6$ *Chandra* position error indicated by the green circle or in the $0\farcs5$ ATCA circle (in red).

4. DISCUSSION

In order to investigate the nature of IGR J17177−3656, we note that IGR J17177−3656 is located in the Galactic plane at $(l, b) = (350\fdg1, 0\fdg51)$. Its X-ray emission together with its quasi-simultaneous radio emission suggests that we are dealing with an X-ray binary, rather than with an active galactic nucleus (AGN) seen through the Galactic plane. From our least absorbed spectrum in Table 1, we obtain for the *unabsorbed* fluxes, relative to *Chandra* normalization, $F_{\rm 3–9\,keV} = 7.5 \times 10^{-11}$ erg cm^{-2} s^{-1} and $F_{\rm 3–200\,keV} = 1 \times 10^{-9}$ erg cm^{-2} s^{-1}. Using the relation found by Merloni et al. (2003) that defines a "fundamental plane" in the three-dimensional ($L_{<10\,\rm keV}$, $L_{\rm R}$, M) space, and our quasi-simultaneous X-ray (unabsorbed 3–9 keV) and radio emission, we see that we would need to place the source at about 100 Mpc to obtain a 3–9 keV luminosity of $\sim 10^{44}$ erg s^{-1}, obtaining an estimated mass of about $4.4 \times 10^4\ M_\odot$ which is too low for an AGN. Placed at 1 Gpc, the source would have a luminosity as high as $L_{\rm X} \sim 10^{46}$ erg s^{-1}, still not reaching $10^6\ M_\odot$ ($4.7 \times 10^5\ M_\odot$), which is extremely unlikely for an AGN scenario.

On the other hand, considering a binary at a distance of 8 kpc would result in an unabsorbed luminosity $L_{\rm 3–9\,keV} = 5 \times 10^{35}$ erg s^{-1} and $L_{\rm 3–200\,keV} = 7 \times 10^{36}$ erg s^{-1} which is compatible with an X-ray binary luminosity.

Although the *Chandra* observation occurred already in the declining phase of the outburst, its flux is comparable to the peak seen by *Swift* (see Figure 1): hence IGR J17177−3656 likely belongs to the so-called class of Very Faint X-ray Transients (VFXT), i.e., transients showing outbursts with low peak luminosity 10^{34}–10^{36} erg s^{-1} in 2–10 keV (Wijnands et al. 2006).[14]

VFXT are believed to be the faintest known accretors and are very likely a non-homogeneous class of sources. It is likely

[14] Indeed even considering the *Swift* peak flux according to Zhang et al. (2011) (occurring on MJD 55636.8), we obtain a non-absorbed $F_{\rm 2–10\,keV} = 8.2 \times 10^{-11}$ erg cm^{-2} s^{-1}, leading to $L_{\rm 2–10\,keV} = 6 \times 10^{35}$ erg s^{-1} at 8 kpc.

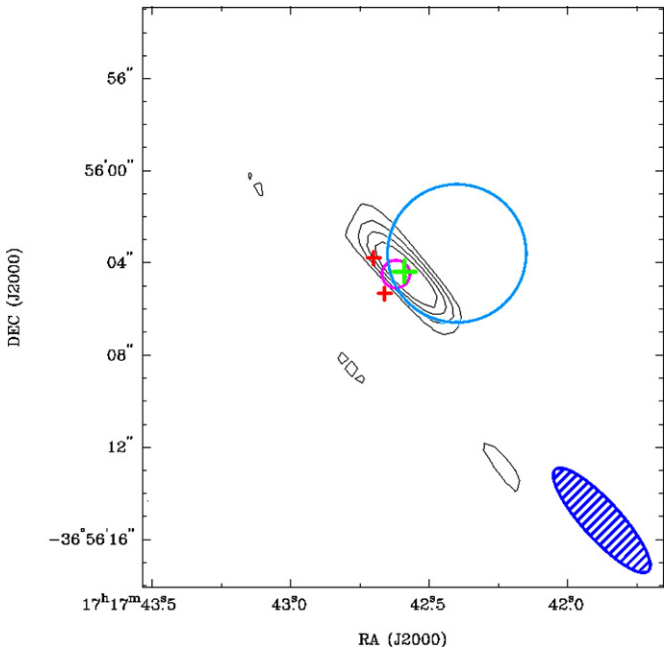

Figure 6. Radio map using the combined ATCA observations of IGR J17177−3656 at 5.5 and 9 GHz (see the text). The green cross represents the fitted position of the ATCA counterpart, the purple circle is the 0.″6 *Chandra* error, the light-blue one is the 3″ *Swift* error, while the red crosses are the two NIR candidates discussed in the text (Torres et al. 2011; Rojas et al. 2011).

that most of them are neutron stars and black holes (BHs) accreting matter from a low-mass companion (Wijnands et al. 2006) and it has been found that a significant fraction of them (∼1/3) have exhibited type-I X-ray bursts (Del Santo et al. 2010, and references therein). This is currently not the case for IGR J17177−3656, and the BH possibility, though more difficult to infer, is still open (see Section 4.2).

4.1. LMXB or HMXB?

In order to speculate over the nature of the companion (hence high-mass X-ray binary, HMXB, versus low-mass X-ray binary, LMXB), we have to consider the K_s limits obtained in quiescence, so that we are not contaminated by the disk X-ray to NIR re-processing, as would be the case for an LMXB. The archival NIR maps studied by Rojas et al. (2011) show that no source was detected within either the *Chandra* or the ATCA radio error circles in 2010 April–October maps, down to a limit of $K_s \sim 18.0$. Using the relation of Predehl & Schmitt (1995), a visual extinction of $A_V = 39.1$ mag is derived from $N_H = 7 \times 10^{22}$ cm^{-2} (Table 1). Assuming a spectral type supergiant Ib (B0.5) with $M_V = -6.8$ and $V - K = -0.75$ (Ducati et al. 2001; i.e., an HMXB), a distance of 8 kpc, and using the extinction law of Cardelli et al. (1989), $A_K/A_V = 0.114$, we obtain an estimated observed $K = 12.92$ that would have been detected in the maps by Rojas et al. (2011) (the NIR emission from an HMXB does not vary dramatically due to its bright stellar emission). Hence in the case of an HMXB hosting a supergiant, to reach the $K \sim 18.0$ limit we would need to place the source at about 83 kpc or more. Given our unabsorbed X-ray flux ($F_{3-200\,keV} = 1 \times 10^{-9}$ erg cm^{-2} s^{-1}), this would result in an X-ray luminosity of about $L_{(3-200\,keV)} \sim 8 \times 10^{38}$ erg s^{-1} from an HMXB placed outside the Galaxy. This scenario, though not impossible, is highly unlikely since such luminosities are too high for HMXBs with the compact object accreting stellar wind.

On the other hand, Be stars (representing the majority of companions in HMXB systems) are main-sequence stars of spectral type between 09 and B2, with a spread in absolute magnitude of nearly 1 mag (see, e.g., Cox et al. 1984). Be X-ray binaries, although dimmer than supergiants, are usually bright NIR sources. The Be phenomenon itself, with the presence of a decretion disk due to fast stellar rotation close to disruption, increases the luminosity of the source, at a level of about $K = 0.25$ mag (Dougherty et al. 1994). To give an example, a normal B0V star (absolute magnitude $M_V = -4.1$) with apparent $K \sim 18$ mag and $A_V = 39.1$ mag would be at nearly 25 kpc, and the disk emission would have the effect of increasing its distance by nearly 3 kpc, placing this star at nearly 28 kpc. This is a substantial distance, for instance in comparison with the faintest ($K_s = 15.75$) and furthest (>8.5 kpc) known candidate BeXRB in the Galaxy, described in Zurita Heras & Chaty (2008). In general, however, distances of HMXBs, hosting both Be and supergiant stars, are usually of the order of a few kpc, due

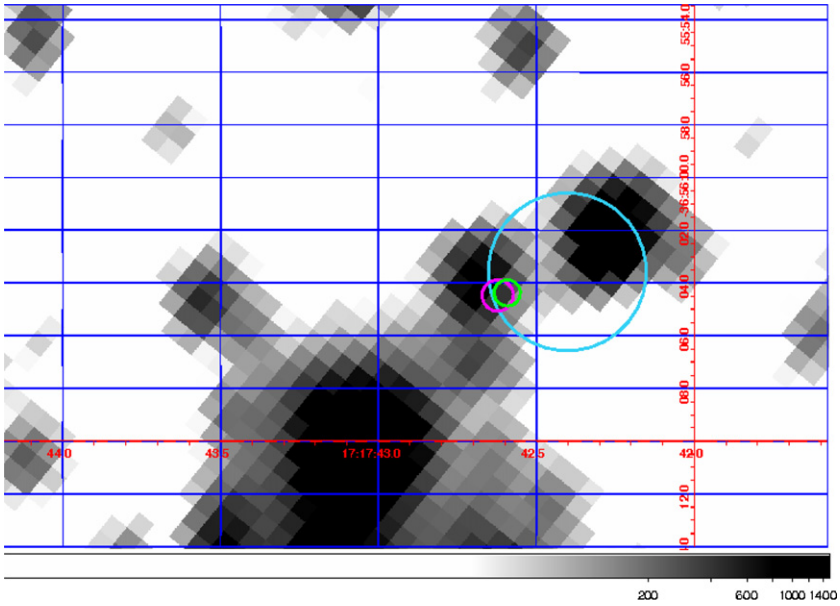

Figure 7. Final averaged K_s image of the field of view around IGR J17177−3656. As in Figure 6, the green circle represents the ATCA position, the purple circle is the *Chandra* error, while the light-blue one is obtained with *Swift*.

to their lower intrinsic X-ray luminosities than LMXBs, and they are distributed mainly toward tangential directions of the Galactic arms (Grimm et al. 2002).

Furthermore, direct accretion through stellar wind—common in HMXBs—should prevent the formation of strong and coherent jets, while the detection of radio emission from IGR J17177−3656 suggests the presence of ejection phenomena, and therefore an LMXB nature filling its Roche lobe and forming an accretion disk.[15]

All these arguments suggest that the HMXB nature can be reasonably ruled out, pointing toward an LMXB nature for IGR J17177−3656. Indeed, assuming a spectral type main-sequence K5 star with $M_V = 7.3$ and $V - K = 2.66$ mag (Ducati et al. 2001; i.e., an LMXB) and a distance of 8 kpc, we would obtain $K \sim 23$ mag, compatible with the non-detection in Rojas et al. (2011), and an X-ray luminosity of about $L_{(3-200\,\mathrm{keV})} = 7 \times 10^{36}$ erg s^{-1} that, though dim, is not exceptional for the LMXB outburst luminosities.

4.2. A Low-mass X-Ray Binary: Geometry and Compact Object

Adding the local and Galactic (ISM) absorbing column densities of Table 1, we observe that we obtain a column density up to about 10 times more than the Galactic average value expected in the source direction, $\sim 1.3 \times 10^{22}$ cm^{-2} (Kalberla et al. 2005). An LMXB does not have an important wind from the companion, that is generally an old K–M-type star, but if it is seen at a high inclination (>60°) it will appear as heavily absorbed due to the material that gets into the line of sight (disk, blob of impact of the accreting matter onto the disk, the companion itself, etc.). This is the case for the dipping, eclipsing, or so-called coronal sources, i.e., sources that exhibit dips, total or partial eclipses in the soft X-ray spectra (e.g., X1822−371, EXO 0748−676, 4U 1624−490; Parmar et al. 1986; White & Holt 1982; Xiang et al. 2009; Díaz Trigo et al. 2006).

In our case, it is difficult to state if we are in the "pure-dipper" scenario (inclination between 60° and 75°) or at higher inclinations (eclipsing or coronal source). We do not see any total eclipse in our data (zero flux) but our soft X-ray observations are either continuous 20 ks (5.5 hr, *Chandra*) or quick snapshots that add up to about 15 ks (*Swift*) which is a small part of a typical LMXB orbital period (typically below 15–20 hr). For such a dim source, we would need to integrate many orbital periods to observe a modulation (dip, eclipse, etc.), but what is clear is that the environment we are observing is not "clean" (high N_H) and it is irregular and patchy (the three rate levels in *Chandra* are not contiguous in time).

We note that the non-variability in the IBIS/ISGRI spectrum together with the absence of total eclipses (albeit the short coverage) could suggest that the Comptonizing region (responsible for the photons above 20 keV) would be extended and wider than the blocking material. Such "coronal" sources are usually known as Accretion Disk Corona sources (ADC), high inclination systems where the accretion disk completely blocks the line of sight to the central source at all orbital phases, but that can still be observed because the corona allows X-rays to be scattered into the line of sight. If this is the case for IGR J17177−3656, then the "true" X-ray flux could be higher. This is very similar to what was obtained by Xiang et al. (2009) on the high inclination LMXB, the so-called Big Dipper, 4U 1624−490, based on a *Chandra* grating observation over the ∼76 ks binary orbit of the source. The continuum spectrum could be modeled using a single $\Gamma \sim 2$ power law partially covered by a local absorber of column density $N_H \sim 8 \times 10^{22}$ cm^{-2} besides the Galactic one, similarly to IGR J17177−3656. Unlike Xiang et al. (2009), our data do not allow us to constrain discrete lines in the spectrum (due to the short exposure and dim source), but we can speculate that the scenario for IGR J17177−3656 could be similar to the Big Dipper case for which Xiang et al. (2009) have shown that X-ray variations are predominantly driven by changes in obscuration, rather than intrinsic variation of the components.

LMXBs are known to produce radio emission, be they hosting a BH or a neutron star. Though BH binaries are known to be more radio-loud, there are clearly some broad similarities in their X–radio coupling, such as the association between X-ray spectral states and the presence of radio emission (Fender 2006; Corbel et al. 2003; Coriat et al. 2011; Migliari & Fender 2006; Paizis et al. 2006). Radio emission can result either from a powerful compact jet in the hard state or from relativistic discrete ejections at spectral state transitions (from hard-intermediate to soft-intermediate state, e.g., Fender 2006). While discrete radio ejections show a radio spectrum with spectral index $\alpha < 0$, compact jets have a flat or slightly inverted spectrum (i.e., $\alpha \gtrsim 0$). In our case, the poorly constrained $\alpha = -0.37 \pm 0.79$ does not allow us to firmly establish the nature of the radio emission; however since IGR J17177−3656 has not shown any important spectral transition but stayed in the hard state, it is likely that the radio emission is associated with compact jets.

The quasi-simultaneous observation and detection of IGR J17177−3656 with *Chandra* and ATCA are very important because besides leading to a constrained source position, they basically rule out the AGN and HMXB nature of the source. Indeed IGR J17177−3656 fits well in the LMXB scenario also from the radio emission point of view (regardless of the inclination). Figure 8, adapted from Coriat et al. (2011), shows the radio luminosity against the 3–9 keV un-absorbed luminosity for a sample of BH candidate LMXBs in the hard state (H 1743−322, GX 339−4, and V404 Cyg) and atoll neutron star LMXBs in the island state (Aql X−1 and 4U 1728−34). The line is the fit to GX 339−4 from S. Corbel et al. (2011, in preparation). IGR J17177−3656 is also shown in the plot. The assumed distance is 8 kpc with an unabsorbed X-ray flux of $F_{(3-9\,\mathrm{keV})} = 7.5 \times 10^{-11}$ erg cm^{-2} s^{-1} (obtained from the least absorbed case) and a radio flux of $F_{(\mathrm{radio})} = 0.2$ mJy. IGR J17177−3656 seems to follow the behavior of the BH candidate LMXB H 1743−322 at low fluxes, when it starts to join the standard correlation of GX 339−4 (Corbel & Tzioumis 2011; Coriat et al. 2011). This could possibly suggest that IGR J17177−3656, that appears also to be too radio bright to be a neutron star LMXB, is a BH candidate in the hard state. We note however that we cannot firmly exclude the neutron star nature of the compact object based on the location of IGR J17177−3656 in Figure 8 alone, since in the aforementioned ADC scenario the observed flux (hence luminosity) could be underestimated. A higher "true" X-ray flux would indeed move the source toward the neutron star populated area.

[15] One could suppose the case of Cyg X−1, which exhibits both an accretion disk and stellar wind, but this source is the only example known in our Galaxy of BH with Roche lobe overflow in a supergiant X-ray binary. In general, HMXBs strictly filling their Roche lobe are likely not observable, since the mass transfer is highly unstable and the accretion should only last for a few thousand years. Instead, there are HMXBs exhibiting Beginning Atmospheric Roche lobe overflow, where the massive star does not fill its Roche lobe, but the stellar wind follows the Lagrange equipotentials, and accumulates, forming an accretion disk (Bhattacharya & van den Heuvel 1991). This situation is more stable, but still rare due to the required configuration of stellar radius, orbital distance, and mass ratio, since we know only three such systems in total, hosting neutron stars: LMC X−4, Cen X−3, and SMC X−1.

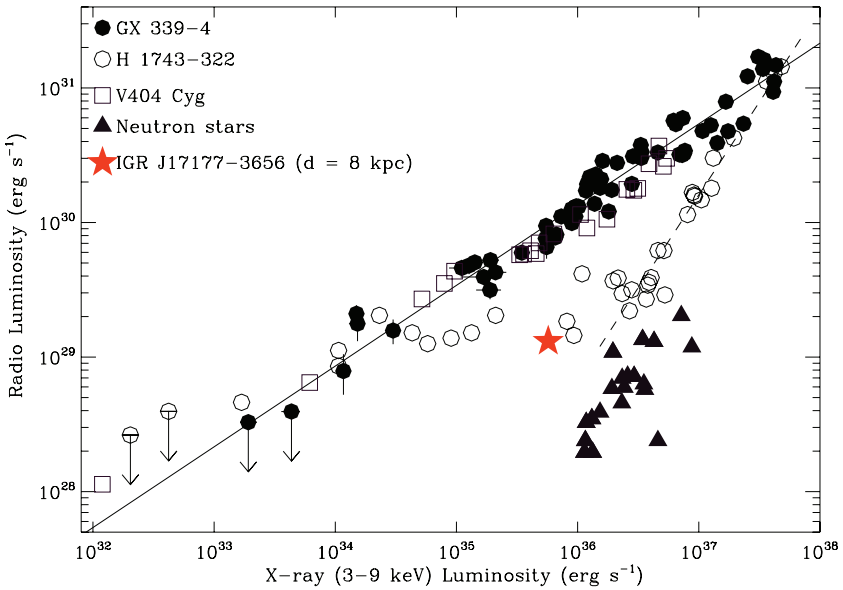

Figure 8. Radio to X-ray luminosity for a sample of black hole and neutron star LMXBs. Adapted from Coriat et al. (2011); see the text for details.
(A color version of this figure is available in the online journal.)

We thank the *Chandra* team for their rapid response in scheduling and delivering the observation, as well as the *INTEGRAL* Science Data Center for their quick and efficient sharing of *INTEGRAL* results.

Partly based on observations with *INTEGRAL*, an ESA project with instruments and science data center funded by ESA member states, Czech Republic and Poland, and with the participation of Russia and the USA. This publication makes use of data products from the Two Micron All Sky Survey, which is a joint project of the University of Massachusetts and the Infrared Processing and Analysis Center/California Institute of Technology, funded by the National Aeronautics and Space Administration and the National Science Foundation. IRAF is distributed by the National Optical Astronomy Observatory, which is operated by the Association of Universities for Research in Astronomy (AURA), Inc., under cooperative agreement with the National Science Foundation. The Australia Telescope is funded by the Commonwealth of Australia for operation as a national Facility managed by CSIRO.

A.P., M.D.S., and P.U. acknowledge financial contribution from the agreement ASI-INAF I/009/10/0. M.D.S. acknowledges the grant from PRIN-INAF 2009 (PI: L. Sidoli). This work was supported by NASA Grant GO1-12054X and partly supported by the Centre National d'Etudes Spatiales (CNES), based on observations obtained with MINE: the Multi-wavelength INTEGRAL NEtwork. J.W. and S.C. acknowledge support from the European Community's Seventh Framework Programme (FP7/2007–2013) under grant agreement number ITN 215212 "Black Hole Universe." J.W. acknowledges support also from the Bundesministerium für Wirtschaft und Technologie through Deutsches Zentrum für Luft- und Raumfahrt Grant 50 OR 0801.

A.P. acknowledges Nicola La Palombara for the generous sharing of his laptop during an emergency, allowing us to trigger our *Chandra* observation in due time, and Lara Sidoli for useful discussions.

REFERENCES

Bhattacharya, D., & van den Heuvel, E. P. J. 1991, Phys. Rep., 203, 1
Burrows, D. N., Hill, J. E., Nousek, J. A., et al. 2005, Space Sci. Rev., 120, 165
Canizares, C. R., Huenemoerder, D. P., Davis, D. S., et al. 2000, ApJ, 539, L41
Cardelli, J. A., Clayton, G. C., & Mathis, J. S. 1989, ApJ, 345, 245
Corbel, S., Nowak, M. A., Fender, R. P., Tzioumis, A. K., & Markoff, S. 2003, A&A, 400, 1007
Corbel, S., & Tzioumis, T. 2011, ATel, 3246
Coriat, M., Corbel, S., Prat, L., et al. 2011, MNRAS, 414, 677
Cox, A., Vauclair, S., & Zahn, J. P. 1984, Mercury, 13, 93
Del Santo, M., Sidoli, L., Romano, P., et al. 2010, MNRAS, 403, L89
Díaz Trigo, M., Parmar, A. N., Boirin, L., Méndez, M., & Kaastra, J. S. 2006, A&A, 445, 179
Dougherty, S. M., Waters, L. B. F. M., Burki, G., et al. 1994, A&A, 290, 609
Ducati, J. R., Bevilacqua, C. M., Rembold, S. B., & Ribeiro, D. 2001, ApJ, 558, 309
Fender, R. 2006, in Compact Stellar X-ray Sources, ed. W. H. G. Lewin & M. van der Klis (Cambridge: Cambridge Univ. Press), 381
Frankowski, A., Ferrigno, C., Bozzo, E., et al. 2011, ATel, 3223
Gehrels, N., Chincarini, G., Giommi, P., et al. 2004, ApJ, 611, 1005
Grimm, H.-J., Gilfanov, M., & Sunyaev, R. 2002, A&A, 391, 923
Hodapp, K. W., Chini, R., Reipurth, B., et al. 2010, Proc. SPIE, 7735, 77351A
Houck, J. C. 2002, in High Resolution X-ray Spectroscopy with XMM-Newton and Chandra, Proc. Int. Workshop held at Mullard Space Science Laboratory, University College London, ed. G. Branduardi-Raymont
Kalberla, P. M. W., Burton, W. B., Hartmann, D., et al. 2005, A&A, 440, 775
Kuulkers, E., Shaw, S. E., Paizis, A., et al. 2007, A&A, 466, 595
Lebrun, F., Leray, J. P., Lavocat, P., et al. 2003, A&A, 411, L141
Merloni, A., Heinz, S., & di Matteo, T. 2003, MNRAS, 345, 1057
Migliari, S., & Fender, R. P. 2006, MNRAS, 366, 79
Morrison, R., & McCammon, D. 1983, ApJ, 270, 119
Paizis, A., Farinelli, R., Titarchuk, L., et al. 2006, A&A, 459, 187
Paizis, A., Nowak, M., Rodriguez, J., et al. 2011, ATel, 3236
Parmar, A. N., White, N. E., Giommi, P., & Gottwald, M. 1986, ApJ, 308, 199
Predehl, P., & Schmitt, J. H. M. M. 1995, A&A, 293, 889
Rojas, A., Masetti, N., & Minniti, D. 2011, ATel, 3275
Sault, R. J., & Killeen, N. 2006, Miriad Users Guide (Australia Telescope National Facility)
Sault, R. J., Teuben, P. J., & Wright, M. C. H. 1995, in ASP Conf. Ser. 77 Astronomical Data Analysis Software and Systems IV, ed. R. A. Shaw, H. E. Payne, & J. J. E. Hayes (San Francisco, CA: ASP), 433
Sault, R. J., & Wieringa, M. H. 1994, A&AS, 108, 585
Torres, M. A. P., Jonker, P. G., Steeghs, D., et al. 2011, ATel, 3241
Ubertini, P., Lebrun, F., Di Cocco, G., et al. 2003, A&A, 411, L131
White, N. E., & Holt, S. S. 1982, ApJ, 257, 318
Wijnands, R., in't Zand, J. J. M., Rupen, M., et al. 2006, A&A, 449, 1117
Wilms, J., Allen, A., & McCray, R. 2000, ApJ, 542, 914
Xiang, J., Lee, J. C., Nowak, M. A., Wilms, J., & Schulz, N. S. 2009, ApJ, 701, 984
Zhang, Y. P., Chen, Y. P., Li, J., et al. 2011, ATel, 3226
Zurita Heras, J. A., & Chaty, S. 2008, A&A, 489, 657